Dirac cones in two-dimensional artificial crystals for classical waves

Jiuyang Lu, Chunyin Qiu,* Shengjun Xu, Yangtao Ye, Manzhu Ke, and Zhengyou Liu*
Key Laboratory of Artificial Micro- and Nano-structures of Ministry of Education and School of Physics and Technology, Wuhan University, Wuhan 430072, China

(Received 7 September 2013; revised manuscript received 21 March 2014; published 4 April 2014)

We present a study on the existence of Dirac cones in two-dimensional phononic crystals. Specifically, we start from the phononic crystals made of rotatable regular hexagonal or triangular rods arranged in a hexagonal lattice. The additional freedom of the rotation enables the crystals with various symmetries. The numerical and experimental band structures manifest consistently that part of the symmetries can support Dirac cones stably, yet the others cannot. The phenomena are explained successfully by the $\mathbf{k}\cdot\mathbf{p}$ perturbation theory combined with symmetry analysis. Based on this theoretical framework, a systemic exploration on symmetry is further performed, which yields a complete summary on the existence of Dirac cones. The conclusion also remains in the other types of artificial crystals for classical waves, either scalar or vectorial ones.

DOI: 10.1103/PhysRevB.89.134302 PACS number(s): 42.70.Qs, 43.20.+g, 63.20.−e

Conic dispersions, originally proposed for relativistic particles based on the Dirac equation [1], have attracted much attention recently since the successful fabrication of graphene, a monolayer of carbon atoms arranged in a honeycomb lattice [2]. This unique energy dispersion leads to fantastic phenomena in electronic transports [3]. The conic dispersion (or Dirac cone) is not limited in atomic crystals. It has been widely observed in two-dimensional (2D) artificial crystals (ACs) for classical waves, such as electromagnetic (EM) waves [4–17] and sound waves [18–21]. Recently, many intriguing wave transport properties associated with conic dispersions have been observed, such as one-way edge modes [4–7], *Zitterbewegung* oscillations [8,9], extremal transmissions [10–13,18], and extinction of coherent backscattering [14,15]. The macroscopic character of the classical waves greatly facilitates the analog study of quantum systems and even provides new insight on the exotic Dirac materials.

Dirac cones are characterized by two indispensable features: the double degeneracy and linear dispersion near the degenerate point (i.e., Dirac point). Both of them depend on the symmetry of the crystal; more specifically, for a concerned Bloch wave vector $\mathbf{k}$, they are closely related to the point group of $\mathbf{k}$ [22,23], which is constituted by a part of the symmetry operations of the crystal point group that transform $\mathbf{k}$ into itself or its equivalent one $\mathbf{k}+\mathbf{g}$, with $\mathbf{g}$ being a reciprocal lattice vector of the crystal. (Note that the terminology "the point group (or symmetry) of wave vector $\mathbf{k}$" does not simply refer to the symmetry of $\mathbf{k}$ in reciprocal space.) Although a great many works manifest the existence of Dirac cones in 2D ACs, they are focused on the graphenelike structures characterized by the C_{3v} symmetry of the corner points in the first hexagonal Brillouin zone (BZ). In view of the excellent tunability in geometric and material parameters, the ACs allow varied crystal symmetries other than the graphenelike structures. A natural question is produced: are there any other crystal symmetries that support Dirac cones? Particularly, can Dirac cones occur at the center of the first BZ [24] (as a more direct analogy to that proposed originally in relativistic quantum mechanics)? In addition, in many cases the vectorial property of the EM or sound waves must be fully taken into account [15,16], which complicates the problem remarkably. Is there an essential difference between the scalar and vectorial wave systems? These questions necessitate a systemic exploration of various crystal symmetries in different types of ACs.

In this paper, we start from 2D phononic crystals (PCs) made of a hexagonal lattice and focus on the BZ corners [classified by inequivalent K- and K'-points, as illustrated in Fig. 1(a)], in which the conic dispersions have already been repeatedly observed [18–21]. To introduce a diversity of the crystal symmetry, the lattice is positioned with rotatable regular hexagonal or regular triangular epoxy rods, as exhibited in Figs. 1(b) or 1(c). For the hexagonal ones, our study exhibits a robust existence of Dirac cones in the BZ corners, irrespective of the orientation of the artificial atoms. For the triangular ones, however, it is observed that only special orientations support Dirac cones. The experimental results agree excellently with the numerical ones. Together with an elegant symmetry analysis based on the group theory, the $\mathbf{k}\cdot\mathbf{p}$ perturbation method is employed to understand the aforementioned phenomena. Furthermore, the study is extended to the other symmetries. It is concluded that the parameter stable (e.g., filling ratio) Dirac cones are protected only by the $C_{3(v)}$ symmetry of the $\mathbf{k}$-point (realizable in the BZ corners of hexagonal lattices positioned with proper building blocks), whereas the parameter unstable ones can occur in more general cases. It is worth pointing out that the theoretical reasoning involves mostly the crystal symmetry, and thereby similar conclusions can be directly made for the other types of classical waves in 2D ACs, even for the complex vectorial elastic waves.

As displayed in Fig. 2, the PC sample consists of a hexagonal array of regular hexagonal or regular triangular rods (of height 1.2 cm, made of epoxy that is acoustically rigid with respect to air). The whole system is tightly sandwiched between the laboratory table and a covering epoxy plate. The parallel gap supports only the fundamental waveguide mode for a wavelength (in air) down to $\lambda = 2.4$ cm, which safely guarantees the experiment system of 2D nature. The acoustic signal is launched from a narrow tube with diameter of 0.8 cm,

*Corresponding authors: cyqiu@whu.edu.cn; zyliu@whu.edu.cn

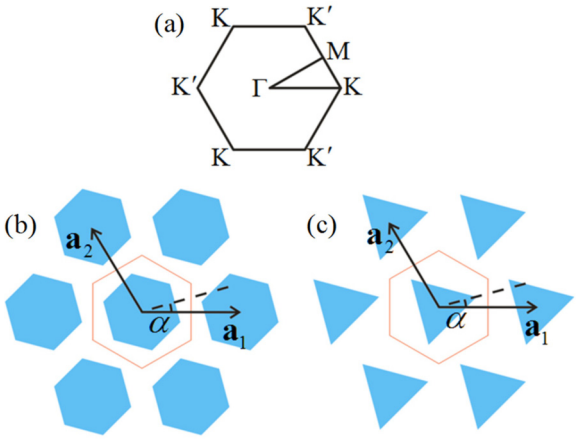

FIG. 1. (Color online) (a) The first BZ of the hexagonal lattice, where several points of high symmetries are marked. (b) Schematic view for the PC consisting of regular hexagonal epoxy rods arranged in a hexagonal lattice, where H' characterizes the orientation of the rod with respect to the fixed lattice (spanned by the primitive vectors $\mathbf{a}_1$ and $\mathbf{a}_2$). (c) Same as (b) but for regular triangular rods.

which mimics a pointlike sound source. After being reflected by a carefully designed parabolic concave mirror, the acoustic wave eventually approximates a plane wave. The interface normal of the PC sample is chosen along ΓK direction. The distribution of the pressure field behind the sample can be scanned by a probe microphone of diameter ~0.7 cm (B&K Type 4187). The acoustic signals sent from the measurement tube and received by the probe microphone are analyzed by a multianalyzer system (B&K Type 3560B), from which both the wave amplitude and phase can be extracted. By reference to the case without a sample, one can obtain the transmission and the phase accumulation across the sample, where the latter provides the directional band structure of the PC [25].

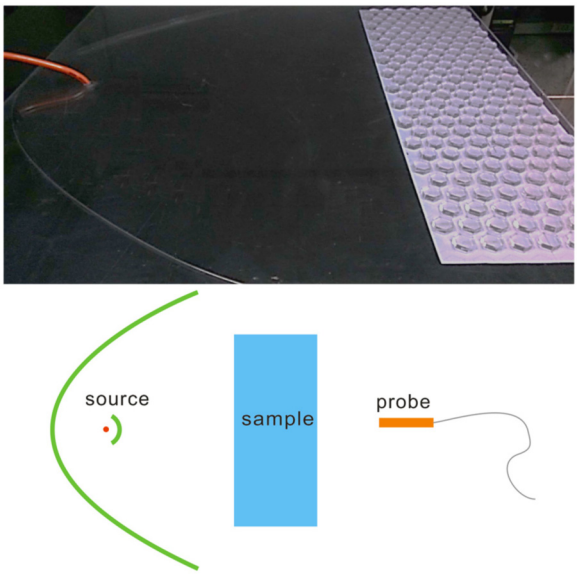

FIG. 2. (Color online) Experimental setup (the upper panel) and its schematic picture (the lower panel).

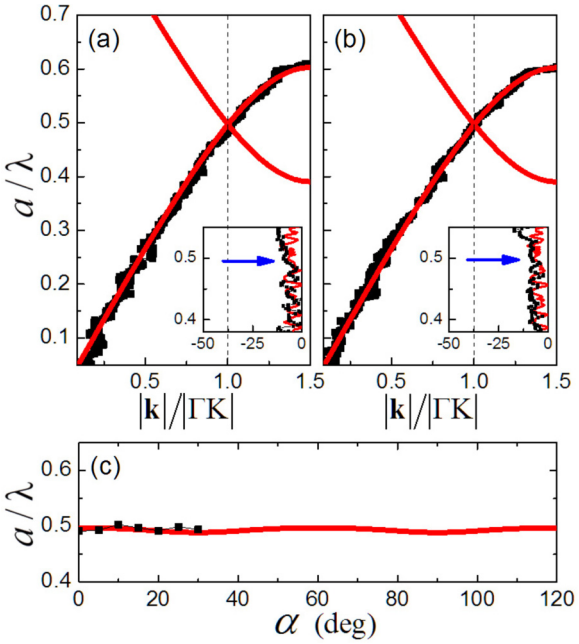

FIG. 3. (Color online) Band structures along ΓK direction for the hexagonal PCs made of regular hexagonal epoxy rods, with the rotation angles $\alpha = 0^o$ (a) and $\alpha = 20^o$ (b). The insets show the corresponding transmission spectra near the Dirac points (denoted by blue arrows), where the horizontal and vertical axes represent the transmission (in decibel scale) and the normalized frequency a/λ, respectively. (c) The angular dependence of the Dirac frequency. Here, the black circles and red lines represent the experimental and numerical results, respectively.

The PC system considered first consists of regular hexagonal epoxy rods, which are of simple shape but with the highest spatial symmetry of the hexagonal lattice. The lattice constant is $a = 4.3$ cm, and the filling ratio of rod is 0.48. Obviously, the PC possesses C_{6v} symmetry when the rod is orientated felicitously by $\alpha = 0^o$. The K-point, however, corresponds to the C_{3v} symmetry since the sixfold rotation transfers it to the inequivalent K'-point (and vice versa). As pointed out in both the natural graphene and ACs, the C_{3v} symmetry of the corner points allows the existence of Dirac cones. This is indeed displayed in Fig. 3(a) by the numerical band structure along the ΓK direction (simulated by the COMSOL package), which exhibits linearly crossed dispersion curves near the K-point (corresponding to $|\mathbf{k}| / |\Gamma K| = 1$). To verify it in an experiment, we have measured the directional band structure. As a whole, the measurement agrees pretty well with the calculation, except for a deaf band (recoiled with negative group velocity) uncoupled with the normal incidence [26]. The absence of the band gap has also been validated by the high transmission (see inset) measured near the frequency of the crossing point. From the gapless band structure, the existence of the Dirac cone surrounding the K-point can be safely concluded, considering the continuities of the band structure in reciprocal space. (This is also numerically verified by the omnidirectional band structure in Fig. 5 in the Appendix). As the rod is rotated arbitrarily, the mirror symmetry breaks and reduces the PC symmetry to C_6 and reduces the symmetry of the K-point to C_3. For comparison, Fig. 3(b) presents

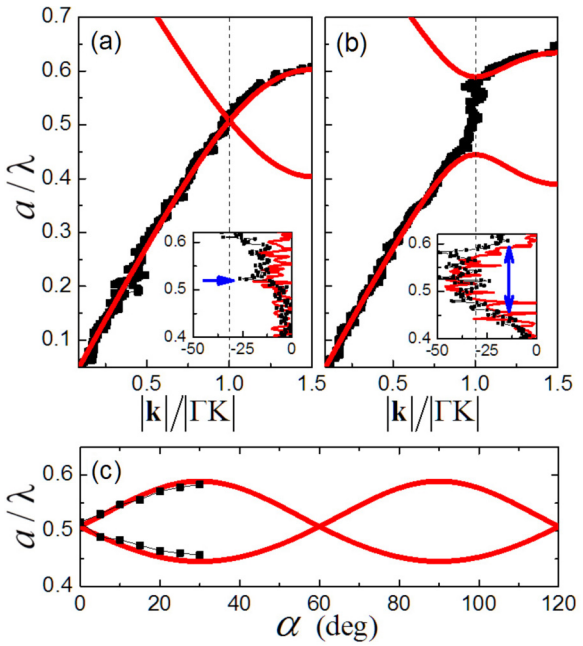

FIG. 4. (Color online) Similar to Fig. 3, but for the PCs made of regular triangular rods with rotation angles $\alpha = 0^o$ (a) and $\alpha = 30^o$ (b), where the insets show the corresponding transmission spectra near the Dirac point or band gap. (c) The angular dependent frequencies for the band edges at the K-point.

similar data as in Fig. 3(a) but for $\alpha = 20^o$. Resembling the case of $\alpha = 0^o$, the numerical and experimental results exhibit consistently the existence of Dirac cones. In fact, our further study states that the conic dispersion is very robust to the rod's orientation, as displayed in Fig. 3(c) by the weak angular dependence of the Dirac frequency [27].

From the above study the C_3 (instead of C_{3v}) symmetry of the K-point might be adequate for the emergence of Dirac cones. To test this conjecture, we reduce the rotation symmetry of the building block and investigate the PC made of regular triangular rods (at a ratio of 0.24). Similarly, we have also calculated and measured the band structures and transmission spectra for various rotation angles. Figure 4(a) provides the results for $\alpha = 0^o$, an orientation associated with C_{3v} symmetry at K-point (consistent with the PC's symmetry). As expected, the data exhibit conic dispersions again. It is much different for $\alpha = 30^o$: as shown in Fig. 4(b), a remarkable frequency gap appears in the band structure [28], within which the transmission is considerably low (see inset). In this case, although the PC has also C_{3v} symmetry, the K-point carries only C_3 symmetry since the mirror operations of the PC cannot transform the K-point into its equivalent ones. In fact, the band gap remains for a general orientation accompanying with C_3 symmetry for both the PC and the K-point. This is manifested clearly in Fig. 4(c) by the angular dependences of the band-edge frequencies, which merge together only if the orientation supports the C_{3v} symmetry of the K-point.

The studies of both the hexagon- and triangle-based PCs state that the C_{3v} symmetry of the K-point can always support Dirac cones, whereas it is not necessary for the C_3 symmetry. Below, together with symmetry analysis, we develop a $\mathbf{k}\cdot\mathbf{p}$ perturbation method [29] to understand these phenomena.

The conic dispersion requires primarily the presence of the double degeneracy, either a deterministic or accidental one. The latter is greatly sensitive to the system parameters. Without details presented here, our further studies show that the aforementioned Dirac cones are robust to the filling ratio of rods and should correspond to the deterministic double degeneracy. For the C_{3v} point group (of $\mathbf{k}$), the 2D irreducible representation is allowed and exactly responsible for the double degeneracy occurring in both the PCs made of hexagonal and triangular rods at some special orientations. For the C_3 point group, however, it can only support three, one dimensional (1D) representations (two of which are complex), which seems contradictory to the stable Dirac cones emerging in the hexagon PC with an arbitrary rotation angle. This paradox can be resolved by considering the extra double degeneracy assisted by time-reversal (TR) symmetry. For the hexagon PC system, in view of the C_6 symmetry of the PC, the rotation operators c_2, c_6, and c_6^{-1} can transform the K-point into its TR counterpart, K'-point, and vice versa; based on Herring's criterion [30], the pair of 1D complex representations can always stick together into a 2D representation and give rise to an extra double degeneracy. It is different for the triangle PC (associated with $C_{3(v)}$ symmetry): there is no group element to relate the inequivalent corner points and thus fails to contribute an extra double degeneracy, which eventually leads to the gap openings at K-point for the PCs with general rod orientations [see Fig. 4(c)].

Now, we verify the linearity of the above conic dispersions near the K-point (see details in the Appendix). The PC system can be described by the generalized eigenproblem

$$H(\mathbf{r})\psi_{\mathbf{k}}(\mathbf{r}) = \omega_{\mathbf{k}}^2\kappa^{-1}(\mathbf{r})\psi_{\mathbf{k}}(\mathbf{r}), \tag{1}$$

where $\psi_{\mathbf{k}}(\mathbf{r})$ denotes the eigenstate associated with the reduced Bloch wave vector $\mathbf{k}$ and eigenfrequency $\omega_{\mathbf{k}}$, and the Hamiltonian $H(\mathbf{r}) = -\nabla\cdot[\rho^{-1}(\mathbf{r})\nabla]$. The parameters $\rho(\mathbf{r})$ and $\kappa(\mathbf{r})$ are the periodically distributed mass density and bulk modulus, respectively. According to the $\mathbf{k}\cdot\mathbf{p}$ perturbation method, the Bloch eigenstate $\psi_{\mathbf{k}}(\mathbf{r})$ vicinal to the K-point can be expanded by a pair of orthonormal eigenstates $\psi_1(\mathbf{r})$ and $\psi_2(\mathbf{r})$, degenerated at the K-point, i.e., $\psi_{\mathbf{k}}(\mathbf{r}) = e^{i\Delta\mathbf{k}\cdot\mathbf{r}}[A_1\psi_1(\mathbf{r}) + A_2\psi_2(\mathbf{r})]$, where $\Delta\mathbf{k}$ characterize the deviation of $\mathbf{k}$ from the K-point. Substituting this linear expansion into Eq. (1), one can establish a perturbation problem

$$\sum_{j=1,2} H'_{ij}A_j = 2\omega_K\Delta\omega A_i, \tag{2}$$

where $H' = \Delta\mathbf{k}\cdot\mathbf{p}$ is the linear perturbation Hamiltonian associated with the vector operator $\mathbf{p} = -i[2\rho^{-1}(\mathbf{r})\nabla + \nabla\rho^{-1}(\mathbf{r})]$ and $\Delta\omega$ is the frequency deviation from that of K-point ω_K. The perturbation Hamiltonian H' can be proved Hermitian and guarantees real eigenvalues. With fully considering the constraints imposed by symmetries, one can establish relationships among the elements of the $\mathbf{p}$ matrix and greatly simplify the form of H'. It is of particular interest that for all the previously mentioned cases with deterministic double degeneracies, the symmetry analysis leads to identical

H', i.e.

$$H' = |\Delta\mathbf{k}|\,|\mathbf{p}_{11}| \begin{pmatrix} \cos\theta & -\sin\theta \\ -\sin\theta & -\cos\theta \end{pmatrix}, \quad (3)$$

where $\mathbf{p}$ is the azimuth angle of $\Delta\mathbf{k}$ with respect to $\mathbf{p}_{11}$. The eigenvalues of H' provide directly the isotropic slopes (i.e., so-called Dirac velocity) $\Delta\omega/|\Delta\mathbf{k}| = \pm|\mathbf{p}_{11}|/2\omega_K$ for the linear dispersion near the K-point, with ω_K being the Dirac frequency.

An important feature that characterizes Dirac cones is the nonzero value (π) of the Berry phase [3], which is expected to be closely connected with various unusual wave transport properties [31–33] (e.g., antilocalization to disorders). By using the eigenvectors derived from the simplified perturbation Hamiltonian, the Berry phase of π can be verified analytically for the aforementioned conic states (see details in the Appendix), consistent with that found previously in 2D ACs [4,5,14,15,19].

The aforementioned study states that, besides the well-known C_{3v} symmetry of the K-point in hexagonal lattices, the C_3 symmetry can also robustly support Dirac cones if associated with the crystal symmetry of C_6. Based on the same theoretical framework, we have further investigated the other high symmetries carrying deterministic double degeneracies, either in the BZ center or BZ corners. In these cases, the constraints from symmetries suppress H' to be zero and exclude the possibility of Dirac cones (see technique details in the Appendix). Our theoretical analysis has also been extended to search Dirac cones induced by accidental double degeneracies (referring to that at a given $\mathbf{k}$-point, the degeneracy can occur only at carefully designed system parameters). The exploration states that such Dirac cones can be realized in the hexagonal BZ corner with C_3 symmetry or in a more general $\mathbf{k}$-point (excluding $\mathbf{k} = \mathbf{g}/2$) carrying C_1 or C_s symmetry (created by more general lattices positioned with proper building blocks). For the latter case, interestingly, the Dirac cones turn out to be tilted and anisotropic (see numerical examples in the Appendix). These accidental Dirac cones also exhibit a Berry phase of π.

Although the PCs for scalar acoustic waves are focused here, the theoretical framework can also be straightforwardly extended to the ACs for other types of classical waves; the procedure in determining the existence of Dirac cones applies well, even if the vectorial property of classical waves is involved, as exemplified by the elastic waves in PCs (see technique details in the Appendix). Our study states that the presence of Dirac cones depends only on the system symmetry, due to the same constraints exerted on the perturbation Hamiltonian. In addition, besides the traditional 2D phononic and photonic crystals made of infinitely long cylinders or holes, the treatment remains valid for the 2D ACs without translational invariance normal to the lattice plane. Particular cases can be referred to 2D periodic arrays of artificial atoms, interacting with planar guiding modes carried by interfaces, cavities [11–13], and plates [21] or interacting with the self-induced guiding modes by wave scattering or hopping. For example, the theory can explain the Dirac cones occurring in a 2D hexagonal array of plasmonic spheres for EM waves [15,16], and also appearing in a 2D hexagonal array of holes drilled on a rigid surface for spoof surface acoustic waves [20], where the latter involves only scalar waves, but the former must consider the vectorial property of EM waves. Therefore, our theory can explain well the existing Dirac cones occurring in various 2D classical ACs. Last, but not least, considering certain common properties in various waves, this study could be useful to enlighten the area of Dirac physics in 2D quantum systems [34]. In fact, a great many 2D crystals have been artificially fabricated, such as nanopatterned heterostructures for 2D electron gases [35,36] and trapped ultracold atoms in optic lattices [37,38], in which various crystal symmetries can be easily realized. New physics phenomena and understanding can be anticipated in the wide parameter regimes inaccessible by natural graphene [39].

TABLE I. A summary on the existence of Dirac cones in various symmetries, where G and $G_{\mathbf{k}}$ represent the point group of the PC and the point group of $\mathbf{k}$, respectively. Note that $\mathbf{k} = \mathbf{g}/2$ (particularly, $\mathbf{k} = 0$, if $\mathbf{g} = 0$) is excluded for the $\mathbf{k}$-point carrying C_1 or C_s symmetry.

G	$G_{\mathbf{k}}$	$\mathbf{k}$	Type
C_{3v} or C_{6v}	C_{3v}	BZ corner	Deterministic
C_6	C_3	BZ corner	Deterministic
C_3 or C_{3v}	C_3	BZ corner	Accidental
Arbitrary	C_1	General $\mathbf{k}$	Accidental
With mirror(s)	C_s	Certain $\mathbf{k}$	Accidental

In conclusion, starting from some specific examples of PCs, we have conducted a systemic study on the existence of Dirac cones in 2D ACs. Now, we approach answers for the questions raised previously: (i) besides the C_{3v} symmetry of the hexagonal BZ corner, linear Dirac cones can also occur in the other symmetries, as summarized in Table I; (ii) Dirac cones cannot occur at the BZ center; (iii) the presence of Dirac cones depends only on the system symmetry, irrelevant to the scalar or vectorial property of waves. As predicted, all of the aforementioned Dirac cones share the same Berry phase of π. This study may also shine light on the artificial structures for matter waves, in which various crystal symmetries different from graphene can be easily realized.

This work is supported by the National Natural Science Foundation of China (Grants No. 11174225, No. 11004155, No. 11374233, and No. J1210061), Open Foundation from State Key Laboratory of Applied Optics of China, the Program for New Century Excellent Talents (NCET-11-0398), and the China Postdoctoral Science Special Foundation (201104491).

APPENDIX

In this appendix, we provide details to support the text. In Sec. A., we establish a theoretical framework for scalar acoustic waves, which effectively combines the k · p perturbation method with symmetry analysis. The detailed exploration on a variety of symmetries is provided in Sec. B., followed with numerical verifications of various conic dispersions in Sec. C. Exemplified by the vectorial elastic waves, extended discussions on the other types of ACs are further presented in Sec. D.

A. Theoretical framework for acoustic waves in PCs

For simplicity, we consider first the acoustic waves propagating in 2D PCs made of pure (isotropic) fluid ingredients. This model can be well applied to the case described in text, given the rigid assumption of epoxy (with respect to the air host).

The propagation of time-harmonic acoustic waves in inhomogeneous media can be described by

$$\kappa(\mathbf{r})\nabla\cdot[\rho^{-1}(\mathbf{r})\nabla\psi(\mathbf{r})]+\omega^2\psi(\mathbf{r})=0, \tag{A1}$$

where $\psi(\mathbf{r})$ represents the pressure field, and $\rho(\mathbf{r})$ and $\kappa(\mathbf{r})$ denote the mass density and compression modulus, respectively. Considering the planar periodicity of the 2D PC in xy-plane, the acoustic wave equation can be rewritten as the eigenproblem

$$H\psi_{\mathbf{k}}(\mathbf{r})=\omega_{\mathbf{k}}^2\kappa^{-1}(\mathbf{r})\psi_{\mathbf{k}}(\mathbf{r}), \tag{A2}$$

where the Hamiltonian $H(\mathbf{r})=-\nabla\cdot[\rho^{-1}(\mathbf{r})\nabla]$ and $\psi_{\mathbf{k}}(\mathbf{r})$ is the eigenstate characterized by reduced Bloch wave vector $\mathbf{k}$ (in the xy plane) and eigenfrequency $\omega_{\mathbf{k}}$.

1. $k\cdot p$ perturbation method

Suppose there is a d-fold degeneracy at $\mathbf{k}$-point. According to the k · p perturbation method [29], the Bloch state $\psi_{\mathbf{k}'}(\mathbf{r})$ vicinal to the degenerate point can be expanded in the (orthogonal) degenerate subspace $\{\psi_i(\mathbf{r})\}$, i.e.,

$$\psi_{\mathbf{k}'}(\mathbf{r})=e^{\mathrm{i}\Delta\mathbf{k}\cdot\mathbf{r}}\sum_{j=1}^{d}A_j\psi_j(\mathbf{r}), \tag{A3}$$

where $\Delta\mathbf{k}=\mathbf{k}'-\mathbf{k}$ and $\{A_i\}$ are coefficients of the linear expansion. The orthogonality of the degenerate eigenstates is defined by $\int\psi_i^*(\mathbf{r})\psi_j(\mathbf{r})\kappa^{-1}(\mathbf{r})d\Omega=\delta_{ij}$, where the integral covers the whole primitive cell and δ_{ij} is the Kronecker delta. Substituting Eq. (A3) into Eq. (A2) and using the orthogonality, one can reformulate the eigenproblem in the degenerate subspace

$$\sum_{j=1}^{d}\left[\omega_{\mathbf{k}}^2\delta_{ij}+\Delta\mathbf{k}\cdot\mathbf{p}_{ij}+|\Delta\mathbf{k}|^2q_{ij}\right]A_j=\omega_{\mathbf{k}'}^2A_i, \tag{A4}$$

where $\mathbf{p}_{ij}=\int\psi_i^*(\mathbf{r})\mathbf{p}\psi_j(\mathbf{r})d\Omega$ and $q_{ij}=\int\psi_i^*(\mathbf{r})q\psi_j(\mathbf{r})d\Omega$, with the vector operator $\mathbf{p}=-\mathrm{i}[2\rho^{-1}(\mathbf{r})\nabla+\nabla\rho^{-1}(\mathbf{r})]$ and the scalar operator $q=1/\rho(\mathbf{r})$. It is easy to prove that the operator $\mathbf{p}$ is Hermitian, i.e., $\mathbf{p}_{ij}=\mathbf{p}_{ji}^*$.

Neglecting the high-order term $|\Delta\mathbf{k}|^2q_{ij}$ and focusing on the linear one, Eq. (A4) reduces to

$$\sum_{j=1}^{d}H'_{ij}A_j=2\omega_{\mathbf{k}}\Delta\omega A_i. \tag{A5}$$

Here, the matrix $H'=\Delta\mathbf{k}\cdot\mathbf{p}$ is the perturbation Hamiltonian of the original degenerate eigenproblem, which is also Hermitian and guarantees the eigenvalue $2\omega_{\mathbf{k}}\Delta\omega$ to be real, with $\Delta\omega=\omega_{\mathbf{k}'}-\omega_{\mathbf{k}}$.

2. Symmetry analysis by group theory

The Hamiltonian $H(\mathbf{r})$ is invariant under certain rotations and reflections. These symmetry operations, determined by specific building blocks positioned in given lattices, together form a point group G of the crystal. According to the group theory, the property of Bloch states is closely related to the so-called point group of the Bloch wave vector $\mathbf{k}$, denoted by $G_{\mathbf{k}}$, which is constituted by a part of symmetry operations of G that transform $\mathbf{k}$ into itself or its equivalent one $\mathbf{k}+\mathbf{g}$, with $\mathbf{g}$ being a reciprocal lattice vector of the crystal [23]. Specifically, $G_{\mathbf{k}}$ coincides G at $\mathbf{k}=0$.

When a group element $R\in G_{\mathbf{k}}$ acts on the crystal, it means that the coordinate variable $\mathbf{r}$ in all functions defined on the crystal changes to $R^{-1}\cdot\mathbf{r}$. Specifically, the action of R transforms the eigenstate $\psi_i(\mathbf{r})$ into $O_R\psi_i(\mathbf{r})=\psi_i(R^{-1}\cdot\mathbf{r})$ through a scalar function operator O_R. According to the group theory, the degenerate eigenstates form a set of basis functions of the representation of $G_{\mathbf{k}}$, and the transformed state can be linearly expanded as $O_R\psi_i(\mathbf{r})=\sum_{j=1}^{d}D_{R,ij}\psi_j(\mathbf{r})$, where D_R is the associated representation matrix of the element R [23]. Now, we study the action of R on the integration $\mathbf{p}_{ij}=\int\psi_i^*(\mathbf{r})\mathbf{p}\psi_j(\mathbf{r})d\Omega$. Under this action, besides the transform of the eigenstate, all material parameters appearing in the vector operator $\mathbf{p}$ are invariant due to the crystal symmetry in direct space, and the gradient operator ∇ transforms into $R^{-1}\cdot\nabla$. Considering that the integration itself is not a function of coordinates and thus invariant to the action, we have

$$\mathbf{p}_{ij}=R^{-1}\cdot\sum_{j=1}^{d}D_{R,mi}^*D_{R,nj}\mathbf{p}_{mn}. \tag{A6}$$

This establishes the relations among the matrix elements $\mathbf{p}_{ij}$, thus simplifying the form of the perturbation Hamiltonian $H'=\Delta\mathbf{k}\cdot\mathbf{p}$.

B. Double degeneracies, Dirac cones, and Berry phases

To investigate the existence of Dirac cones, below we focused on the case of the double degeneracy ($d=2$) for various symmetries. Unless specifically stated otherwise, the point group mentioned in the following refers to $G_{\mathbf{k}}$.

The double degeneracies can be produced automatically by the 2D planar point groups C_{3v} and C_{6v} in hexagonal lattices and C_{4v} in square lattices, which carry 2D irreducible representations. Without mirror symmetries, the point groups C_3, C_6, and C_4 do not carry 2D irreducible representations but can still support deterministic double degeneracies: according to Herring's criterion [30], a pair of conjugate 1D complex representations often stick together into a 2D complex representation. [The exception is the C_3 point group at the hexagonal BZ corner if it is associated with $C_{3(v)}$ symmetry in direct space. A specific example can be referred to the PC made of rotated regular triangular rods, as featured by the remarkable band gap; see Fig. 4(b) in text.]

The double degeneracies can also be realized accidentally by a pair of 1D representations, if the crystal parameters are tailored carefully.

1. Deterministic double degeneracies and Dirac cones

Consider first the point groups C_{3v} and C_3 at the hexagonal BZ corners. As will be shown below, both can generate Dirac cones.

(i) The point group C_{3v} includes six independent elements: the identity, the rotations by $\beta = \pm 2\pi/3$, plus a set of equivalent reflections. The reflections depend on the explicit selection of coordinates, while the rotations do not. For each rotation operation, the 2D irreducible representation can be expressed as $D_R = \begin{pmatrix} \cos\beta & -\sin\beta \\ \sin\beta & \cos\beta \end{pmatrix}$ [23], which mathematically equals the corresponding rotation matrix R in this case. By substituting R and D_R into Eq. (A6), the relationships among $\mathbf{p}_{ij}$ can be established: $\mathbf{p}_{22} = -\mathbf{p}_{11}$, $\mathbf{p}_{12} = \mathbf{p}_{21}$ and $\mathbf{p}_{12} = \begin{pmatrix} 0 & 1 \\ -1 & 0 \end{pmatrix} \cdot \mathbf{p}_{11}$. These relations state that only one vector variable is independent; for convenience, we choose the diagonal element $\mathbf{p}_{11}$, which is real due to the Hermiticity of $\mathbf{p}$. Accordingly, the perturbation Hamiltonian can be simplified as

$$H' = |\Delta\mathbf{k}|\,|\mathbf{p}_{11}| \begin{pmatrix} \cos\theta & -\sin\theta \\ -\sin\theta & -\cos\theta \end{pmatrix}, \tag{A7}$$

where θ is the azimuth angle of $\Delta\mathbf{k}$ with respect to $\mathbf{p}_{11}$. The corresponding eigenvalues $2\omega_K \Delta\omega = \pm|\Delta\mathbf{k}||\mathbf{p}_{11}|$ directly provide the angular-independent slopes $\Delta\omega/|\Delta\mathbf{k}| = \pm|\mathbf{p}_{11}|/2\omega_K$ for the linear dispersion near the K-point. This explains the Dirac cones emerging in Figs. 3(a) and 4(a), where the PCs have C_{6v} and C_{3v} symmetries in direct space, associated with C_{3v} symmetry at the K-point (see text). (In principle, the reflection should be further considered to simplify the perturbation Hamiltonian; however, it only specifies the orientation of $\mathbf{p}_{11}$ and offers nothing new to the analysis of the slopes.)

(ii) The point group C_3 has three independent elements (i.e., the identity and rotations by $\beta = \pm 2\pi/3$) and support only three 1D representations, two of which are complex ones. According to Herring's criterion [30], if (and only if) the crystal has C_6 symmetry in direct space, the pair of 1D complex representations can stick together and contribute a double degeneracy, where the representation matrix of the rotation element turns out to be $D'_R = \begin{pmatrix} e^{i\beta} & 0 \\ 0 & e^{-i\beta} \end{pmatrix}$. Note that this representation is equivalent to that of C_{3v} case (i.e., $D_R = S D'_R S^{-1}$ with $S = \frac{1}{\sqrt{2}}\begin{pmatrix} i & -i \\ 1 & 1 \end{pmatrix}$) and gives rise to identical perturbation Hamiltonian in Eq. (A7). This explains the Dirac cones emerging in Figs. 3(b) for the PC made of rotated regular hexagonal rods.

For the point groups C_{3v} and C_3 at the hexagonal BZ center, the symmetry analyses yield the same perturbation Hamiltonian as in Eq. (A7). However, the sole (Hermitian) variable $\mathbf{p}_{11}$ turns out to be zero as a consequence of real eigenstates [40]. The zero eigenvalues of H' correspond to vanishing slopes of the dispersion and exclude the possibility of the Dirac cones.

For the point group C_{6v} (or C_6) that occurs only in the hexagonal BZ center, it cannot support Dirac cones since the constraints exerted by the subgroups C_{3v} (or C_3) have already caused H' to be null.

It is also easy to rule out Dirac cones for the point groups C_{4v} and C_4, which can occur in both of the BZ center and BZ corners of the square lattices. These symmetries possess an operation of twofold rotation, associated with the representation matrix identical to its rotation matrix. Substituting the matrices into Eq. (A6), it yields immediately $\mathbf{p}_{ij} = 0$ and $H' = 0$. This simple procedure (in excluding Dirac cones) can also be applied to the case of point groups C_{6v} and C_6.

TABLE II. Existence of deterministic Dirac cones.

G	$G_{\mathbf{k}}$	$\mathbf{k}$	Existence
C_{3v} or C_{6v}	C_{3v}	BZ corner	o
C_6	C_3	BZ corner	o
$C_{3(v)}$	$C_{3(v)}$	BZ center	x
$C_{6(v)}$	$C_{6(v)}$	BZ center	x
$C_{4(v)}$	$C_{4(v)}$	BZ center	x
$C_{4(v)}$	$C_{4(v)}$	BZ corner	x

As a summary, Table II provides a list for the existence of deterministic Dirac cones in various symmetries, where "o" and "x" represent positive and negative, respectively.

2. *Accidental double degeneracies and Dirac cones*

The double degeneracy can be generated accidentally by a pair of 1D representations, where the 2D representation matrix is simply a direct sum of the two 1D ones. In the following, we analyze the situations successively according to the symmetry.

(i) Consider first a general $\mathbf{k}$-point at arbitrary lattices. There is no constraint of symmetry exerted on the perturbation Hamiltonian $H' = \Delta\mathbf{k} \cdot \mathbf{p}$. In general, the eigenvalues $2\omega_K \Delta\omega = \frac{1}{2}[\Delta\mathbf{k} \cdot (\mathbf{p}_{11} + \mathbf{p}_{22}) \pm \sqrt{|\Delta\mathbf{k} \cdot (\mathbf{p}_{11} - \mathbf{p}_{22})|^2 + 4|\Delta\mathbf{k} \cdot \mathbf{p}_{12}|^2}]$ give rise to anisotropic and tilted linear conic dispersions, with the tilted angle determined by the orientation of $\mathbf{p}_{11} + \mathbf{p}_{22}$. Note that $\mathbf{k} = \mathbf{g}/2$ should be excluded, as explained below. In such special $\mathbf{k}$-points (particularly, $\mathbf{k} = 0$, if $\mathbf{g} = 0$), the eigenstates can always be chosen as real functions [41]. This enforces $\mathbf{p}_{ij}$ to be pure imaginary and thus leads to $\mathbf{p}_{11} = \mathbf{p}_{22} = 0$, considering the Hermiticity of the vectorial operator $\mathbf{p}$. Therefore, the eigenvalues reduce to $\pm|\Delta\mathbf{k} \cdot \mathbf{p}_{12}|$, which is dependent on the orientation of $\Delta\mathbf{k}$ and strongly anisotropic. The eigenvalues even become zero as $\Delta\mathbf{k}$ is perpendicular to $\mathbf{p}_{12}$, which leads to a parabolic dispersion along this special orientation when the higher order perturbation is involved.

(ii) For the point group of C_s, where the ensemble of such $\mathbf{k}$ forms special line(s) in the reduced BZ, the conclusions in (i) still hold since the mirror symmetry only specifies the orientation of $\mathbf{p}_{ij}$ (accordingly, it enables the Dirac cones with the same symmetry).

(iii) For the point group of $C_{2(v)}$ that occurs only at $\mathbf{k} = \mathbf{g}/2$, the possibility of Dirac cones can be directly excluded according to a similar reasoning in (i).

(iv) For the point groups with higher rotational symmetries, i.e., $C_{n(v)}$ with $n \geqslant 3$, occurring in the BZ center or corners of the hexagonal or square lattices, categorized discussions are made as following. (1) Involving 1D real representations only: in these cases, the 2D representation can be described by the diagonal matrix associated with elements either $+1$ or -1. According to Eq. (A6), we have

$$R \cdot \mathbf{p}_{ij} = \mathbf{p}_{ij} \text{ or } R \cdot \mathbf{p}_{ij} = -\mathbf{p}_{ij}. \tag{A8}$$

The rotation invariance of the n-fold enforces directly $\mathbf{p}_{ij} = 0$, and thus $H' = 0$. This excludes the existence of Dirac cones. (2) Involving 1D complex presentations: this occurs only in the C_3 symmetry of the hexagonal BZ corners, where Herring's criterion fails to create the deterministic double degeneracy if associated with $C_{3(v)}$ symmetry in direct space. For the degeneracy created by the pair of 1D complex representations together, linear conic dispersions should emerge since the 2D representation matrix is totally identical to that of the deterministic case. The accidental hybridization of a 1D real representation and a 1D complex representation can also contribute Dirac cones: using the 2D representation matrix $D_R = \left(\begin{smallmatrix} 1 & 0 \\ 0 & e^{i\beta} \end{smallmatrix}\right)$, the perturbation Hamiltonian can be simplified into

$$H' = |\Delta\mathbf{k}|\,|\mathbf{p}_{12}| \begin{pmatrix} 0 & e^{i\theta} \\ e^{-i\theta} & 0 \end{pmatrix}, \tag{A9}$$

leading to isotropic slope $\Delta\omega/|\Delta\mathbf{k}| = \pm|\mathbf{p}_{12}|/2\omega_K$. Therefore, conic dispersions can be generated by the accidental double degeneracy only if the 1D complex presentation is involved. A specific example can be referred to the 2D PCs made of regular triangular rods, in which the filling ratio of rods is carefully selected for a given orientation, as will be shown in Fig. 7.

As a summary, Table III provides a list for the existence of accidental Dirac cones in various symmetries.

TABLE III. Existence of accidental Dirac cones.

G	$G_{\mathbf{k}}$	$\mathbf{k}$	Existence
Arbitrary	C_1	General $\mathbf{k}$	o
With mirror(s)	C_s	Certain $\mathbf{k}$	o
$C_{2(v)}$, $C_{4(v)}$, $C_{6(v)}$	$C_{2(v)}$	$\mathbf{k} = \mathbf{g}/2$	x
C_3	C_3	BZ center	x
C_3, C_{3v}	C_3	BZ corner	o
C_6	C_3	BZ corner	x
C_{3v}	C_{3v}	BZ center	x
C_{3v}, C_{6v}	C_{3v}	BZ corner	x
C_{4v}	C_{4v}	BZ center/corner	x
C_{6v}	C_{6v}	BZ center	x

3. *Berry phases of the Dirac cones*

The Berry phase [42], an extra phase factor emerging after a dynamic quantum system undergoes an adiabatic loop, has significant influence on the wave transport properties. In the following, we derive the Berry phase for the conic state $\psi_{\mathbf{k}}$, evolving adiabatically along a $\mathbf{k}$-contour surrounding the Dirac point. The Berry phase can be evaluated by the formula

$$\gamma = i \oint \left[\int \psi_{\mathbf{k}}^* \nabla_{\mathbf{k}} \psi_{\mathbf{k}} d\Omega \right] \cdot d\mathbf{k}, \tag{A10}$$

which requires the derivability of the eigenstate $\psi_{\mathbf{k}}$ with respect to $\mathbf{k}$ [43]. For simplicity, we choose the integral path to be an arbitrary small circle centered on the Dirac point. Using the orthonormality of the degenerate eigenstates, Eq. (A10) can be reduced to

$$\gamma = i \int_0^{2\pi} d\theta \sum_{j=1,2} A_j^* \frac{\partial}{\partial\theta} A_j. \tag{A11}$$

Naturally, Eq. (A11) requires the derivability of the eigenvector with respect to the parameter θ. In the following, we show that all of the aforementioned Dirac cones carry the same Berry phase of π.

For the Dirac cones occurring in the hexagonal BZ corners, either deterministically or accidentally, from the perturbation Hamiltonian, we can analytically derive the normalized eigenvectors for the upper and the lower Dirac cones. Specifically, the perturbation Hamiltonian in Eq. (A7) provides eigenvectors $(A_1, A_2) = e^{i\theta/2}(-\cos\theta/2, \sin\theta/2)$ and $(A_1, A_2) = e^{i\theta/2}(\sin\theta/2, \cos\theta/2)$, and the perturbation Hamiltonian in Eq. (A9) provides $(A_1, A_2) = (e^{i\theta}/\sqrt{2}, 1/\sqrt{2})$ and $(A_1, A_2) = (-e^{i\theta}/\sqrt{2}, 1/\sqrt{2})$. In both cases, Eq. (A11) gives the Berry phase $\gamma = \pi$ for each cone.

For the Dirac cones accidentally occurring at a more general $\mathbf{k}$-point associated with C_1 or C_s symmetry, without tedious derivation presented here, we have also verified the Berry phase of π by virtue of the analytic eigenvectors.

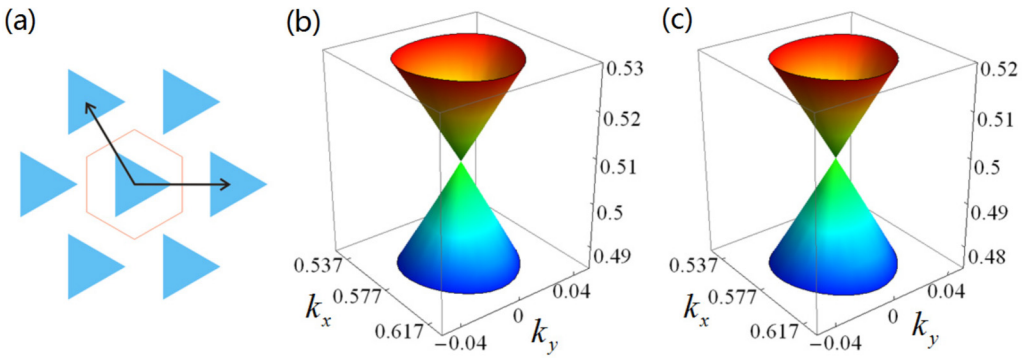

FIG. 5. (Color online) Parameter stable Dirac cones for the hexagonal PCs made of regular triangular rods, where the special rod orientation is chosen to enable the PC with C_{3v} symmetry in both direct space and the K-point, as displayed in (a). The variation of the filling ratio from 0.240 (a) and 0.265 (b) shifts the normalized Dirac frequency from 0.508 to 0.499.

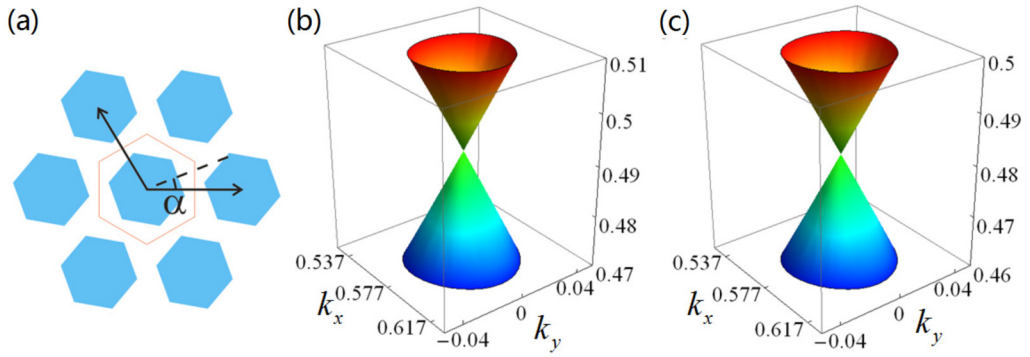

FIG. 6. (Color online) Parameter stable Dirac cones for the hexagonal PCs made of regular hexagonal rods, where a general rod orientation ($\alpha = 20^o$) is chosen to enable the PC with C_6 symmetry in direct space and with C_3 symmetry at the K-point, as displayed in (a). The variation of the filling ratio from 0.480 (a) and 0.530 (b) shifts the normalized Dirac frequency from 0.492 to 0.481.

C. Numerical verifications for various Dirac cones

Here, we provide numerical verifications (simulated by the COMSOL package) for various Dirac cones discussed in Appendix Sec. B, as summarized in Tables II and III. For simplicity, here we consider PCs made of rigid rods placed in a fluid matrix, in which only the geometry of rods is involved. In each system, two different filling ratios are employed to illustrate the parameter stability of the Dirac cones. It should be pointed out that the Dirac cones can emerge in various frequencies and appear in pairs (or multipairs) in the reduced BZ; for clarity, in each case only one Dirac cone (with the lowest frequency) is displayed around the corresponding Dirac point.

Figures 5–8 display the Dirac cones produced by various symmetries, which are realized in hexagonal lattices positioned with building blocks of different shapes or orientations. (The property of the Dirac cone produced by C_1 symmetry resembles that of C_s symmetry; thus, only the latter is provided.) The characteristics of these Dirac cones are briefly summarized as follows: (i) Shapes of the Dirac cones: the Dirac cones displayed in Figs. 5–7 are isotropic (due to the rotational symmetry of the system) and associated with conic axes vertical to the **k**-plane; in contrast, the Dirac cones in Fig. 8 are anisotropic, associated with tilted conic axes. (ii) Parameter stability of Dirac cones: arising from deterministic double degeneracies, the Dirac cones exhibited in Figs. 5 and Fig. 6 are stable to the filling ratio, while those in Figs. 7 and 8, corresponding to accidental double degeneracies, are sensitive to the filling ratio, associated with either gap opening (Fig. 7) or shift of the Dirac point in **k**-space (Fig. 8).

D. Extensions to the other types of classical waves

1. *Vectorial elastic waves in 2D PCs*

Here, we consider elastic waves propagating in 2D PCs. Compared with the above acoustic systems, the most remarkable difference lies in the vectorial property of elastic waves. The propagation of elastic waves in inhomogeneous (isotropic) media are governed by this equation [44]

$$(\lambda+\mu)\nabla(\nabla\cdot\mathbf{u})+\mu\nabla^2\mathbf{u}+\nabla\lambda(\nabla\cdot\mathbf{u})+\nabla\mu\times(\nabla\times\mathbf{u}) +2(\nabla\mu\cdot\nabla)\mathbf{u}=-\rho\omega^2\mathbf{u}, \quad \text{(A12)}$$

where $\mathbf{u}(\mathbf{r})$ represents the vectorial displacement field and $\lambda(\mathbf{r})$ and $\mu(\mathbf{r})$ are Lame's constants. For elastic media with 2D planar periodicity, the in-plane propagation of the elastic waves can be described by the eigenproblem

$$H(\mathbf{r})\mathbf{u}_\mathbf{k}(\mathbf{r})=\omega_\mathbf{k}^2\rho(\mathbf{r})\mathbf{u}_\mathbf{k}(\mathbf{r}), \quad \text{(A13)}$$

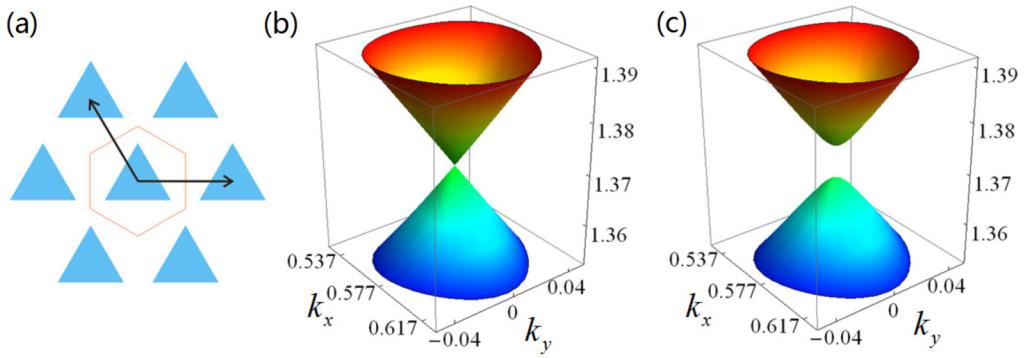

FIG. 7. (Color online) Parameter unstable Dirac cones for the hexagonal PC made of regular triangular rods, where the special rod orientation is chosen to enable the PC with C_{3v} symmetry in direct space and with C_3 symmetry at the K-point, as displayed in (a). The corresponding filling ratios are 0.169 and 0.173 in (b) and (c), respectively; the former induces Dirac cones at the normalized frequency 1.371, whereas the latter opens a band gap.

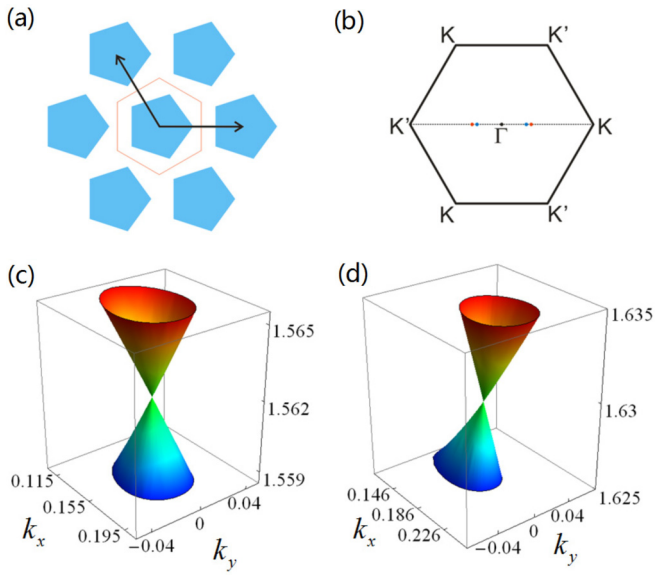

FIG. 8. (Color online) Parameter unstable Dirac cones for the hexagonal PC made of regular pentagonal rods, where the special orientation is chosen to enable the PC with C_s symmetry in direct space, as displayed in (a), and to enable a line of the **k**-point (marked by dashed line) with C_s symmetry. The corresponding filling ratios are 0.484 and 0.532 in (c) and (d), which support Dirac cones at **k**-points denoted by the red and blue points in the first BZ. Specifically, the perturbation of the filling ratio changes the normalized Dirac frequency from 1.562 to 1.630 and shifts the **k**-point from (0.155, 0) to (0.186, 0).

where $H = -[(\lambda+\mu)\nabla\nabla\cdot + \mu\nabla^2 + \nabla\lambda\nabla\cdot + \nabla\mu\times\nabla\times + 2\nabla\mu\cdot\nabla]$ corresponds to the Hamiltonian operator associated with Bloch eigenstate $\mathbf{u_k}(\mathbf{r})$.

Again, for a d-fold degeneracy at **k**-point, the eigenstate in the neighborhood $\mathbf{u}_{\mathbf{k}'}(\mathbf{r})$ can be expressed in the degenerate subspace $\{\mathbf{u}_i(\mathbf{r})\}$, i.e., $\mathbf{u}_{\mathbf{k}'}(\mathbf{r}) = e^{i\Delta\mathbf{k}\cdot\mathbf{r}}\sum_{j=1}^{d} A_j\mathbf{u}_j(\mathbf{r})$. Substituting it into Eq. (A13) and using the orthogonality $\int \mathbf{u}_i^*(\mathbf{r})\cdot\mathbf{u}_j(\mathbf{r})\rho(\mathbf{r})d\Omega = \delta_{ij}$, the eigenproblem turns out to be

$$\sum_{j=1}^{d}\left[\omega_{\mathbf{k}}^2\delta_{ij} + \Delta\mathbf{k}\cdot\mathbf{p}_{ij} + \Delta\mathbf{k}\Delta\mathbf{k}:q_{ij}\right]A_j = \omega_{\mathbf{k}'}^2 A_i, \quad \text{(A14)}$$

where the scalar operator is $q_{ij} = \int(\lambda+\mu)\mathbf{u}_i^*\mathbf{u}_j + \mu(\mathbf{u}_i^*\cdot\mathbf{u}_j)I\,d\Omega$ and the vectorial operator $\mathbf{p}_{ij} = -i\int\mathbf{\Lambda}_{ij}d\Omega$ with

$$\mathbf{\Lambda}_{ij} = (\lambda+\mu)(\mathbf{u}_i^*\nabla\cdot\mathbf{u}_j + \mathbf{u}_i^*\cdot\nabla\mathbf{u}_j) + 2\mu(\nabla\mathbf{u}_j)\cdot\mathbf{u}_i^* + \nabla\lambda\cdot\mathbf{u}_i^*\mathbf{u}_j + \mathbf{u}_i^*\mathbf{u}_j\cdot\nabla\mu + (\mathbf{u}_i^*\cdot\mathbf{u}_j)\nabla\mu.$$

The linear approximation in Eq. (A14) brings the following to a perturbation problem with identical form to Eq. (A5), that is, $\sum_{j=1}^{d} H'_{ij}A_j = 2\omega_{\mathbf{k}}\Delta\omega A_i$.

Similar to the procedure employed in Appendix Sec. A, the perturbation Hamiltonian $H' = \Delta\mathbf{k}\cdot\mathbf{p}$ can be simplified by symmetry analysis. The only difference from the above scalar field case is that now the action of a group element R transforms the vector eigenstate $\mathbf{u}_i(\mathbf{r})$ into $O_R\mathbf{u}_i(\mathbf{r}) = R\cdot\mathbf{u}_i(R^{-1}\cdot\mathbf{r})$, but not simply $O_R\mathbf{u}_i(\mathbf{r}) = \mathbf{u}_i(R^{-1}\cdot\mathbf{r})$, considering the vectorial property of the displacement field. It is of particular interest that the relations among the matrix elements $\mathbf{p}_{ij}$ can be proved to be $\mathbf{p}_{ij} = R^{-1}\cdot\sum_{j=1}^{d} D^*_{R,mi}D_{R,nj}\mathbf{p}_{mn}$, which is exactly the same as that of the acoustic case in Eq. (A6). This eventually gives rise to a universal judgment on the existence of Dirac cones for any given system symmetry, irrespective of the type of sound fields.

2. *Further discussions*

So far, we have studied 2D PCs for both the acoustic and elastic waves. Extensions can be easily made for 2D ACs propagating with the other types of scalar and vectorial classical waves, such as shallow water waves and EM waves. In particular, the scalar wave theory can be straightforwardly applied to the EM waves in traditional 2D photonic crystals, which consist of 2D periodic arrays of infinitely long cylinders or holes in the host media; in this case, the translational invariance in the z direction decouples the EM waves into TM and TE modes, both of which can be handled by a simple mapping with the acoustic systems.

It is also noteworthy that in both discussions of acoustic and elastic PCs, the translational invariance in the z direction is not prerequisite. Besides the traditional 2D phononic and photonic crystals, the treatment remains valid as well for the 2D ACs without z invariance. Therefore, our theory can explain well the Dirac cones occurring in various 2D classical ACs (e.g., the hexagonal array of plasmonic spheres [15,16], where the vectorial property of EM waves must be considered).

[1] See, for example, J. D. Bjorken and S. D. Drell, *Relativistic Quantum Mechanics* (McGraw-Hill, New York, 1964).

[2] K. S. Novoselov, A. K. Geim, S. V. Morozov, D. Jiang, Y. Zhang, S. V. Dubonos, I. V. Grigorieva, and A. A. Firsov, Science **306**, 666 (2004); K. S. Novoselov, A. K. Geim, S. V. Morozov, D. Jiang, M. I. Katsnelson, I. V. Grigorieva, S. V. Dubonos, and A. A. Firsov, Nature (London) **438**, 197 (2005).

[3] A. H. Castro-Neto, F. Guinea, N. M. R. Peres, K. S. Novoselov, and A. K. Geim, Rev. Mod. Phys. **81**, 109 (2009) and references therein.

[4] F. D. M. Haldane and S. Raghu, Phys. Rev. Lett. **100**, 013904 (2008); S. Raghu and F. D. M. Haldane, Phys. Rev. A **78**, 033834 (2008).

[5] T. Ochiai and M. Onoda, Phys. Rev. B **80**, 155103 (2009).

[6] Y. Poo, R. X. Wu, Z. Lin, Y. Yang, and C. T. Chan, Phys. Rev. Lett. **106**, 093903 (2011).

[7] M. C. Rechtsman, J. M. Zeuner, Y. Plotnik, Y. Lumer, D. Podolsky, F. Dreisow, S. Nolte, M. Segev, and A. Szameit, Nature (London) **496**, 196 (2013); A. B. Khanikaev, S. H. Mousavi, W.-K. Tse, M. Kargarian, A. H. MacDonald, and G. Shvets, Nat. Mater. **12**, 233 (2013).

[8] X. Zhang, Phys. Rev. Lett. **100**, 113903 (2008).

[9] Q. Liang, Y. Yan, and J. Dong, Opt. Lett. **36**, 2513 (2011).

[10] R. A. Sepkhanov, Y. B. Bazaliy, and C. W. J. Beenakker, Phys. Rev. A **75**, 063813 (2007).

[11] S. R. Zandbergen and M. J. A. de Dood, Phys. Rev. Lett. **104**, 043903 (2010).

[12] S. Bittner, B. Dietz, M. Miski-Oglu, P. Oria Iriarte, A. Richter, and F. Schäfer, Phys. Rev. B **82**, 014301 (2010); S. Bittner, B. Dietz, M. Miski-Oglu, and A. Richter, *ibid.* **85**, 064301 (2012).

[13] R. A. Sepkhanov, J. Nilsson, and C. W. J. Beenakker, Phys. Rev. B **78**, 045122 (2008).

[14] R. A. Sepkhanov, A. Ossipov, and C. W. J. Beenakker, Europhys. Lett. **85**, 14005 (2009).

[15] G. Weick, C. Woollacott, W. L. Barnes, O. Hess, and E. Mariani, Phys. Rev. Lett. **110**, 106801 (2013).

[16] D. Han, Y. Lai, J. Zi, Z-Q. Zhang, and C. T. Chan, Phys. Rev. Lett. **102**, 123904 (2009).

[17] J. L. Garcia-Pomar, A. Cortijo, and M. Nieto-Vesperinas, Phys. Rev. Lett. **100**, 236801 (2008); M. Bellec, U. Kuhl, G. Montambaux, and F. Mortessagne, *ibid.* **110**, 033902 (2013).

[18] X. Zhang and Z. Liu, Phys. Rev. Lett. **101**, 264303 (2008).

[19] J. Mei, Y. Wu, C. T. Chan, and Z.-Q. Zhang, Phys. Rev. B **86**, 035141 (2012).

[20] D. Torrent and J. Sánchez-Dehesa, Phys. Rev. Lett. **108**, 174301 (2012).

[21] D. Torrent, D. Mayou, and J. Sánchez-Dehesa, Phys. Rev. B **87**, 115143 (2013).

[22] E. P. Wigner, Gött. Nachr. **31**, 546 (1932).

[23] J. Cornwell. *Group Theory in Physics*, Vol. 1 (Academic Press, New York, 1984).

[24] Though linearly crossed dispersions can be accidentally observed in the BZ center, they are always mixed with an additional flat band, associated with remarkably different properties from those emerging in graphene [19]. Literature can be referred to, e.g., X. Huang, Y. Lai, Z. H. Hang, and C. T. Chan, Nat. Mater. **10**, 582 (2011); F. Liu, Y. Lai, X. Huang, and C. T. Chan, Phys. Rev. B **84**, 224113 (2011); K. Sakoda, Opt. Express **20**, 3898 (2012); **20**, 25181 (2012).

[25] S. Yang, J. H. Page, Z. Liu, M. L. Cowan, C. T. Chan, and P. Sheng, Phys. Rev. Lett. **88**, 104301 (2002).

[26] K. Sakoda, Phys. Rev. B **52**, 7982 (1995).

[27] The experimental result is presented only from 0° to 30° considering the sixfold rotational symmetry and even symmetry about $\alpha = 30°$. A treatment is also employed in Fig. 4(c) for the PC made of triangle rods.

[28] Beyond the numerical prediction, the practically measured phase accumulation contributes a sharply increasing dispersion curve near the K-point. Essentially, this frequency range corresponds to a band gap, in which the real part of the wave vector is exactly the value of the K-point, see, e.g., X. Ao and C. T. Chan, Phys. Rev. B **80**, 235118 (2009).

[29] J. C. Slonczewski and P. R. Weiss, Phys. Rev. **109**, 272 (1958).

[30] C. Herring, Phys. Rev. **52**, 361 (1937).

[31] T. Ando and T. Nakanishi, J. Phys. Soc. Jpn. **67**, 1704 (1998); T. Ando, T. Nakanishi and R. Saito, *ibid.* **67**, 2857 (1998).

[32] Y. Zhang, Y.-W. Tan, H. L. Stormer, and P. Kim, Nature (London) **438**, 201 (2005); F. V. Tikhonenko, A. A. Kozikov, A. K. Savchenko, and R. V. Gorbachev, Phys. Rev. Lett. **103**, 226801 (2009).

[33] D. Xiao, M. Chang, and Q. Niu, Rev. Mod. Phys. **82**, 1959 (2010).

[34] Although the present theory cannot apply universally in all 2D quantum systems, it generally holds for simple systems with negligible spin-orbital couplings and electron correlations.

[35] M. Gibertini, A. Singha, V. Pellegrini, M. Polini, G. Vignale, A. Pinczuk, L. N. Pfeiffer, and K. W. West, Phys. Rev. B **79**, 241406(R) (2009).

[36] K. K. Gomes, W. Mar, W. Ko, F. Guinea, and H. C. Manoharan, Nature (London) **483**, 306 (2012).

[37] S.-L. Zhu, B. Wang, and L.-M. Duan, Phys. Rev. Lett. **98**, 260402 (2007).

[38] L. Tarruell, D. Greif, T. Uhlinger, G. Jotzu, and T. Esslinger, Nature (London) **483**, 302 (2012).

[39] See a recent review article and references therein. M. Polini, F. Guinea, M. Lewenstein, H. C. Manoharan, and V. Pellegrini, Nat. Nanotechnol. **8**, 625, (2013).

[40] For the case of C_{3v} symmetry, the real group representation D_R enables that the basis functions can always be chosen as real functions due to the TR symmetry $\psi^*_{\mathbf{k}} = \psi_{-\mathbf{k}}$. This is also true in the case of C_3 symmetry after a similar transformation $D_R = SD'_RS^{-1}$.

[41] In the case of $\mathbf{k} = \mathbf{g}/\mathbf{2}$, equivalent to $\mathbf{k} = -\mathbf{k} + \mathbf{g}$, the eigenstates $\psi_{\mathbf{k}}(\mathbf{r})$ can always be chosen as real functions, since $\psi_{-\mathbf{k}}(\mathbf{r}) = \psi_{\mathbf{k}}(\mathbf{r})$ and $\psi_{-\mathbf{k}}(\mathbf{r}) = \psi^*_{\mathbf{k}}(\mathbf{r})$.

[42] B. Simon, Phys. Rev. Lett. **51**, 2167 (1983); M. V. Berry, Proc. R. Soc. London, Ser. A **392**, 45 (1984).

[43] J. Zak, Phys. Rev. Lett. **62**, 2747 (1989).

[44] F. C. Karal and J. B. Keller, J. Acous. Soc. Am. **31**, 694 (1958).